Brooks, B.E., and Beckermann, C., "Prediction of Burn-on and Mold Penetration in Steel Casting Using Simulation," in Proceedings of the 60th SFSA Technical and Operating Conference, Paper No. 5.3, Steel Founders' Society of America, Chicago, IL, 2006.

PREDICTION OF BURN-ON AND MOLD PENETRATION IN STEEL CASTING USING SIMULATION

Brandon E. Brooks[1] and Christoph Beckermann[2]

[1]Graduate Research Assistant and [2]Professor, Department of Mechanical and Industrial Engineering, The University of Iowa, Iowa City, Iowa 52242, USA

Abstract

Burn-on and penetration defects in steel casting are principally caused by localized over-heating of the sand mold or cores. Such over-heating can cause liquid metal to compromise the mold surface and entrain onto the surface of the mold. A method has been developed to predict likely burn-on and penetration defect locations as part of a standard casting simulation. The method relies on determining, from simulation results, the locations where the mold is above a certain critical temperature. The critical temperature is generally above the temperature at which the steel is fully solidified. By measuring the time periods during which these locations in the mold are above the critical temperature, burn-on and penetration defects can be predicted. The method is validated through comparison with previous experimental data. Several parametric studies are conducted to investigate the sensitivity of the predictions to the choice of the critical temperature, the interfacial heat transfer coefficient between the steel and the mold, the pouring temperature, and the mold material. The results of three case studies are presented where burn-on or penetration defects observed on production steel castings are successfully predicted.

Introduction

Burn-on (also known as burned-on-sand or burnt-on-sand) and metal penetration are common surface defects encountered in sand casting of steel. The Glossary of Foundry Terms [1] defines burned-on sand as "A misnomer usually indicating metal penetration into sand resulting in a mixture of sand and metal adhering to the surface of a casting. Sand adhering to the surface of the casting which [sic] is extremely difficult to remove. This condition may be due to soft molds, poor sand compaction, insufficient mould coating (graphite) paint, or high pouring temperature." The repair or cleaning of burn-on and penetration defects after casting shakeout is not only costly, but can result in considerable delays in casting production. Although efforts have been made to understand the factors that lead to the formation of burn-on and penetration defects, there is currently no tool available to predict their occurrence in a reliable manner. With such a tool, the casting design cycle may be shortened and overall production efficiency may be increased.

Burn-on is a casting defect where liquid metal fills the voids in the sand mold or core without displacing the grains, causing sand, mold wash, or oxides to adhere to the casting surface. The adherents will only be defined as 'burn-on' if they are so strongly ingrained into the casting surface that the surface must be blasted clean. Penetration is considered a

more severe form of burn-on, and penetrated sand must generally be chipped or ground off the casting surface.

Burn-on is caused by liquid steel at the mold-metal interface penetrating shallowly into the mold. Typically, this occurs when the metal at the mold-metal interface stays hot enough for a sufficient amount of time to partially decompose the binder or the mold wash, while remaining partially liquid. Only then can the metal flow into the mold sand. The amount of time that is required for a burn-on defect to occur is unknown. However, the locations that have the greatest probability of experiencing burn-on are those where the metal adjacent to the mold-metal interface remains partially liquid for the longest period of time. These locations, as a rule, tend to be in sharp corners, under risers, next to thick sections of castings, and on the surface of thin cores [2]. There, the mold tends to heat above the solidification temperature of the steel and remain at a high temperature for a relatively long period of time. Clearly, to understand burn-on defects, the interfacial region of the mold where the metal meets the sand must be analyzed.

Penetration is quite similar to the burn-on defect, in that the presence of partially liquid metal at the mold-metal interface and local over-heating of the mold are necessary conditions for the defect to occur. However, penetration is different from burn-on in that it is more difficult to clean because metal penetrates deeper into the mold. Thus, penetrated sand must be ground or chipped off. The depth of the penetration defect is limited by the temperature of the mold away from the casting surface. Since the temperature of the mold usually decreases away from the mold-metal interface, the flowing metal will solidify, thereby stopping the penetration [3]. Therefore, the entire volume of the mold must be analyzed to know not only where on the surface penetration is most likely to occur, but also to determine to what depth into the mold penetration is likely to reach.

Studies have been performed to understand both qualitatively and quantitatively the factors that cause burn-on and metal penetration [2-10]. Svoboda [4] showed that burn-on and penetration are caused by a combination of three modes. The first such mode is liquid-state penetration of metal into the inter-granular voids of the mold. Liquid-state penetration is governed by capillary forces and head height pressure: when the head height pressure is greater than the surface tension resistive force, metal can penetrate into the mold. The second mode of penetration is vapor-state penetration into the mold. The metallic vapor penetrates the mold and subsequently condenses into liquid and then solidifies. The solidified metal changes the surface tension properties, thereby aiding in further liquid-state penetration described as the primary mode of penetration. The third mode found by Svoboda is chemical reaction penetration, where complex oxides are formed by the alloying elements, mold washes, and sand. Svoboda suggested methods of reducing void sizes and changing chemistries of washes and sands to reduce the instances of penetration and burn-on defects.

Richards and Monroe [3] showed that, in fact, the capillary pressure and head height do aggravate penetration instances. They showed that penetration and burn-on are most likely to occur at the hottest locations on the casting surface, and that the depth of

penetration is governed by the thermal profile found in cores and molds. Richards and Monroe also showed that pouring temperature has little effect on instances of penetration because the pouring superheat is only a small fraction of the absolute temperature. They found that proper coating, use of ventilation, and properly placed chromite and zircon sand can reduce penetration. Chromite and zircon sands are particularly beneficial in reducing penetration defects because of their relatively high thermal diffusivity, which tends to reduce local over-heating. The partially solid metal was described as having an increased apparent viscosity. They suggest that 'dendritic lock-up,' at which the partially solid metal is no longer able to flow, occurs at a solid fraction of approximately 60%.

Researchers at the University of Alabama, Tuscaloosa [5-7], devised a method of predicting penetration depth by considering mechanical penetration forces (both head height and capillary forces), dynamic penetration forces (pouring velocity), and the permeability of the sand. Their predictive equation, which was implemented in an Excel® Spreadsheet, was shown to accurately predict penetration depths at individually chosen locations. Richards et al. [8] showed that the type of sand, and specifically the reclamation process used by the foundry, makes the largest difference in reducing instances of burn-on and penetration. In summary, the previous research suggests a number of contributing factors that affect burn-on and penetration. Aside from Ref. [5-7], the studies offer mostly qualitative information regarding the effect of various casting variables and the likely locations for burn-on or penetration defects to occur.

The current study shows how thermal analysis of the mold-metal interface and of the mold (including cores) can be used to accurately locate burn-on and penetration defects. The present method identifies the areas of localized over-heating by performing a standard casting simulation and recording the times the predicted temperatures are above a certain critical temperature. These time duration results are then visualized on the surface of the casting or in the mold.

This paper is divided into five sections. The present simulation methodology is explained in the next section. A detailed comparison with experimental data from Richards et al. [8] is presented in the third section. In addition, parametric studies are performed to investigate the sensitivity of the results to the choice of the critical temperature, the interfacial heat transfer coefficient, the pouring temperature and the type of mold material. The results of three industrial case studies are shown in the fourth section. The final section summarizes the conclusions from this study.

Method

There are numerous factors that contribute to burn-on and penetration defects, as mentioned in the Introduction. However, factors such as mold wash application and mold compaction cannot easily be accounted for in a quantitative manner. Therefore, it was decided to solely focus on the thermal effects. The principle interest of this study is to find the locations that have the highest probability of burn-on and penetration by calculating the times that the interface between the mold and the metal (for burn-on) and the mold (for penetration) stay above some, as of yet unknown, temperature. This

temperature is referred to as the "critical temperature" ($T_{critical}$ on figures) in this study and must generally be above the temperature at which the metal fully solidifies. Standard casting simulation is used to calculate the temperatures everywhere in the mold and metal and, then, to determine the times the temperatures are above the critical temperature.

Description of the Burn-on Prediction. The prediction of burn-on is based on the time that both the temperature of the mold and the temperature of the metal at the interface between the two materials are above the critical temperature. The mold and the metal at the interface are generally at different temperatures because of the presence of a small air gap that forms during solidification of a casting. This is illustrated schematically in Fig. 1. The interfacial air gap acts as an insulator, keeping the steel hotter or the mold cooler. In a casting simulation, the effect of the air gap on the heat transfer is typically modeled by specifying an interfacial heat transfer coefficient. This heat transfer coefficient can be a constant or a temperature dependent function.

When obtaining the metal and mold interfacial temperatures from a casting simulation, care must be taken to interpolate the temperatures to the location of the interface, since they are often only predicted at discrete locations in the metal and the mold away from the air gap. As shown in Fig. 1, the time both interfacial temperatures are above the critical temperature is then measured. This time period is referred to as the "burn-on time" in the present study. The burn-on times are obtained everywhere on the mold-metal interface and can be visualized as different colors on the surface of the casting using the post-processor of the casting simulation software. Since the metal at the interface is usually hotter than the mold, the mold temperature variation actually determines the burn-on time. Note that in many instances, the interfacial temperature of the mold will never be above the critical temperature; then, the burn-on time is simply assigned a value of zero. The regions on the surface of the casting with the longest times above the critical temperature can be expected to most likely experience a burn-on defect. That being said, a large predicted burn-on time (relative to the casting solidification time) does not ensure that such a defect will indeed occur. The present method must be used in the context of the casting under consideration, and the role of the other factors mentioned in the Introduction (such as head height and mold wash) must not be forgotten.

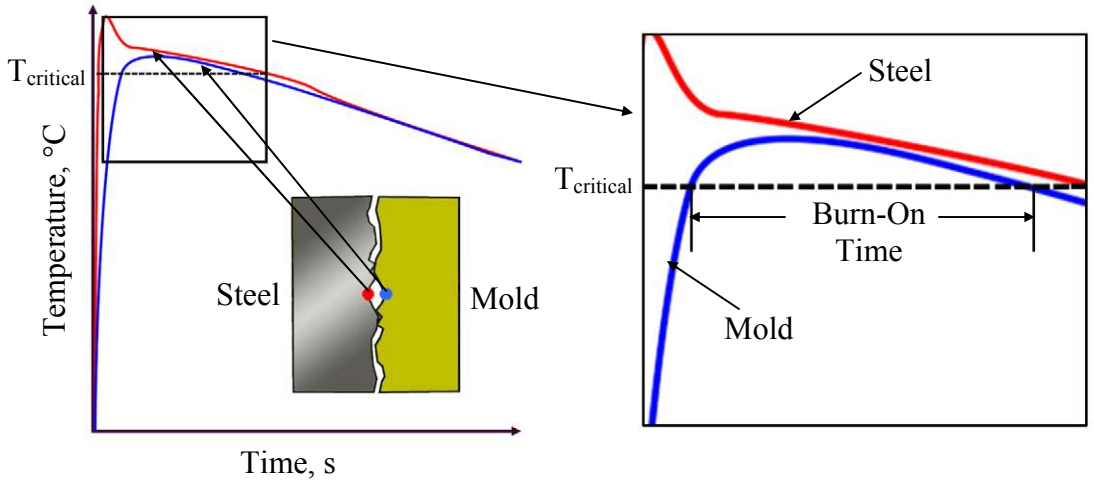

Figure 1. Schematic of the method used to determine the burn-on time from the predicted temperature variations at the mold-metal interface.

Description of the Penetration Prediction. The prediction of penetration is quite similar to that for burn-on. However, the time above the critical temperature is determined everywhere in the mold (including the cores), rather than solely at the mold-metal interface. A schematic illustration of how the penetration times are measured from the predicted temperature variations in the mold is shown in Fig. 2. As in the burn-on prediction, locations in the mold that never reach the critical temperature are assigned a penetration time of zero. Finite penetration times are plotted as different colors inside the mold using the post-processor of the casting simulation software. They indicate likely regions for a penetration defect to occur. In particular, the likely depth of penetration, away from the casting surface into the mold, can be visualized in this manner.

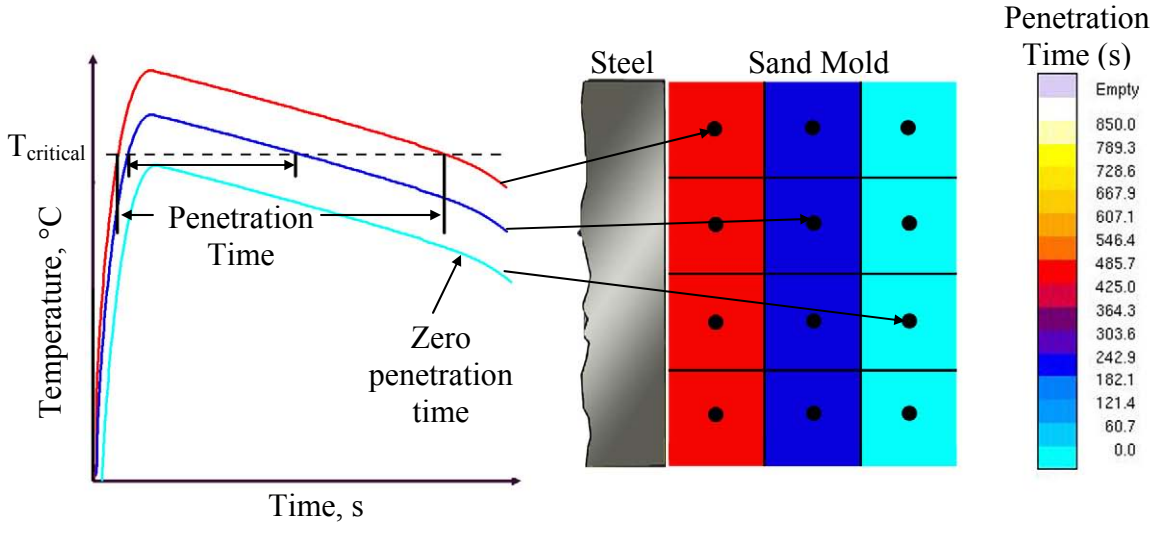

Figure 2. Schematic of the method used to determine the penetration time from the predicted temperature variations in the mold.

Figure 3 illustrates the primary difference between the present burn-on and penetration predictions. If the temperature gradient in the mold near the mold-metal interface is very shallow, the predicted penetration times adjacent to the interface will be similar in magnitude to the burn-on times. On the other hand, if the temperature gradient is steep, the two times will be quite different, and the penetration time near the mold-metal interface can be equal to zero even if the burn-on time is finite. Of course, sufficiently far away from the mold-metal interface the penetration times predicted in the mold are usually equal to zero.

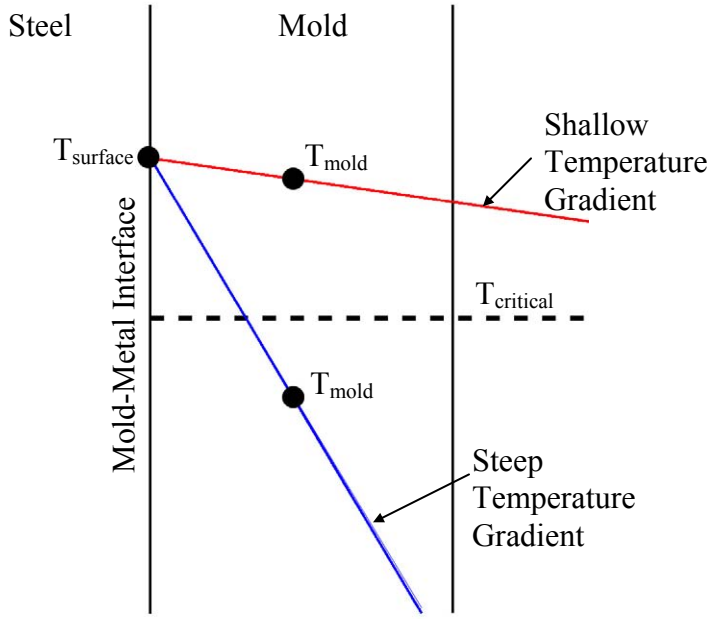

Figure 3. Schematic illustration of the differences in the burn-on and penetration predictions near the casting surface that can be caused by different temperature gradients in the mold.

V-Block: Comparison with Experiments and Parametric Studies

The present method for predicting burn-on and penetration defects is validated by comparison with experimental results obtained by Richards et al. [8] for a casting referred to as the V-block. Since an appropriate value for the critical temperature is not known currently, a parametric study is performed to investigate the sensitivity of the predictions to this temperature. A likely range for the critical temperature is identified. Since there is a relatively large uncertainty in the value of the interfacial heat transfer coefficient used in casting simulations, and the value of this coefficient can be expected to strongly affect the burn-on and penetration predictions, a second parametric study is presented to explore this effect. A third parametric study is conducted to explore the effect of the pouring temperature, since it has been reported to potentially affect the occurrence of burn-on and penetration defects and is often not know to great accuracy. Finally, a fourth parametric

study investigates the effect of different mold materials on the burn-on and penetration predictions.

Review of V-Block Experiments [8]. The experimental casting used by Richards et al. [8] was a V-block made of CF-8C stainless steel in a polyurethane no-bake (PUNB) sand mold (referred to as "furan" in the present study). The dimensions are provided in Fig. 4. The casting was 8.625" long by 7.25" high, with a gross pouring weight of about 151 pounds (including the 4" tall by 6" diameter riser). The casting was designed to have a sharp internal corner, located under a large riser, surrounded by relatively thick sections. Thus, the burn-on or penetration defects always appeared in the "notched" area under the riser (Fig. 5).

As shown in Table 1, the experiments were executed in a full factorial with four different parameters: sand (new or reclaimed), compaction (vibration or hand), work-time/strip (immediate or delay), and coating (flow or brush). All data not reported in Ref. [8] were obtained directly from the authors of that paper. The extent of burn-on or penetration was quantified by measuring the area on the casting surface where the defects occurred. The defect area had approximately the shape of a folded ellipse (see Fig. 5). No distinction was made between burn-on and penetration. The area was determined by measuring the total length, l, of the defect along the notch and its height, h, from the center of the notch to the lowest point along the side of the notch. Then, the defect area, A, is given by:

$$A = \pi\left(\frac{h \cdot l}{2}\right) \tag{1}$$

The measured length and height, and calculated area data is summarized in Table 1. A statictical analysis of the data revealed that, of all the test variables, only the type of sand ("new" or thermally reclaimed sand and mechanically reclaimed sand) had a significant effect on the measured burn-on or penetration areas in these experiments [8]. The averages of the measured defect areas for the two types of sand, as well as the average of all defect areas, together with the corresponding standard deviations, are provided in Table 2. It can be seen that the measured areas for thermally reclaimed ("new") sand are considerably below those for mechanically reclaimed sand.

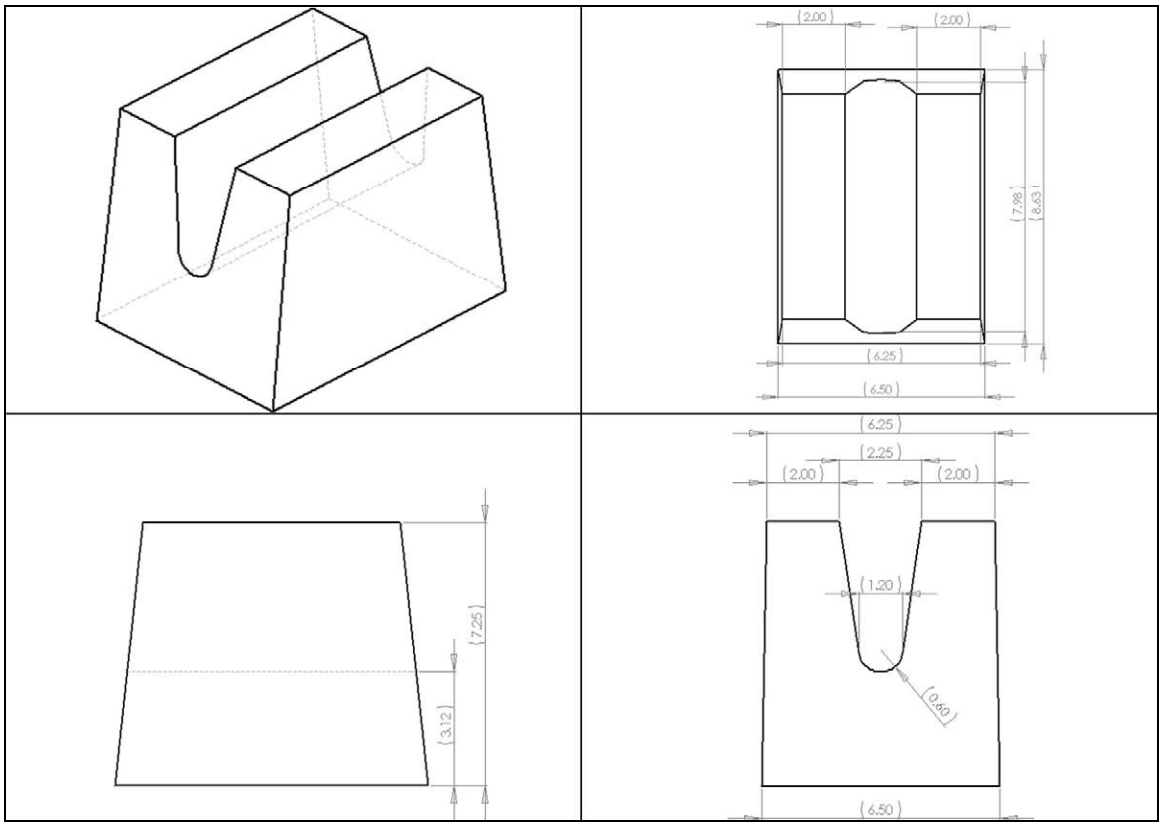

Figure 4. Dimensions of the V-block (shown inverted – drag side up, without direct pour riser) [8].

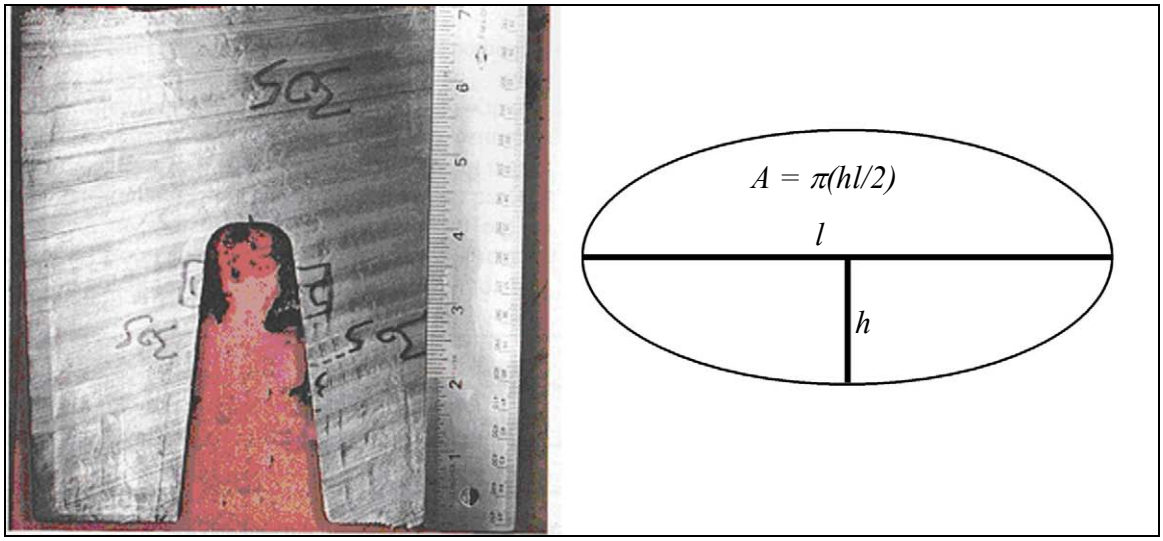

Figure 5. Left: Picture of a slice of the experimental V-block casting with a burn-on or penetration defect area of 17.00 in^2 [8]. Right: Method for measuring the elliptical defect area on the casting surface.

Table 1. Measured burn-on or penetration defect lengths, heights, and areas for the V-block from the experiments of Richards et al. [8].

Length, in	Height, in	Area, in^2	Work time/Strip	Compaction	Sand	Coating
1.4	1.49	3.27	Immediate	Vibration	New	Flow
2.99	3.24	15.21	Immediate	Vibration	New	Brush
1.84	1.07	3.1	Delay	Vibration	New	Flow
1.82	1.69	4.83	Delay	Vibration	New	Brush
5	1.97	15.5	Immediate	Hand	New	Flow
3.09	0.94	4.57	Immediate	Hand	New	Brush
2.78	2.01	8.8	Delay	Hand	New	Flow
3.02	1.01	4.81	Delay	Hand	New	Brush
4.92	2.02	15.64	Immediate	Vibration	Reclaim	Flow
4.69	2.2	16.18	Immediate	Vibration	Reclaim	Brush
4.34	2	13.66	Delay	Vibration	Reclaim	Flow
4.65	2.33	17	Delay	Vibration	Reclaim	Brush
4.24	2.9	19.34	Immediate	Hand	Reclaim	Flow
3.26	1.49	7.62	Immediate	Hand	Reclaim	Brush
3.26	1.34	6.85	Delay	Hand	Reclaim	Flow
4.32	2.12	14.35	Delay	Hand	Reclaim	Brush

Table 2. Averages of measured burn-on or penetration defect areas.

	Area, in^2	Standard Deviation, in^2
Thermally Reclaimed ("New") Sand	7.51	5.14
Mechanically Reclaimed Sand	13.83	4.22
Aggregate Average	10.18	5.66

Simulation Procedure. A solid model of the V-block casting was created and imported into the casting simulation software*. A picture of the casting that was simulated is shown in Fig. 6, together with the riser and insulation. In the simulation, properties available for CF-8M steel were used, because the ones for CF-8C steel were not available. Due to the similarity in the chemical composition of these alloys, small differences in the properties between these two alloys are not expected to significantly affect the burn-on and penetration predictions. For the V-block results presented in this section, the mold filling process was not simulated, primarily because the pour temperatures in the experiments were not reported in Ref. [8]. Instead, a pour temperature

* MagmaSoft® was used in the present study; however, the present method could be used with any casting simulation software.

was estimated, and the temperature drop of the steel during filling was accounted for by choosing a somewhat lower value for the initial temperature of the steel in the mold with which the simulations were started.

All parameters that were chosen for the baseline simulation case are listed inside the box in Fig. 7. The value of 1000 W/m^{2}K used for the (constant) interfacial heat transfer coefficient represents a reasonable first estimate for sand casting of steel. Figure 7 also shows the solid fraction vs. temperature curve used in the V-block simulations. The temperature associated with 45% solid (1405°C) was used as the baseline critical temperature, $T_{critical}$.

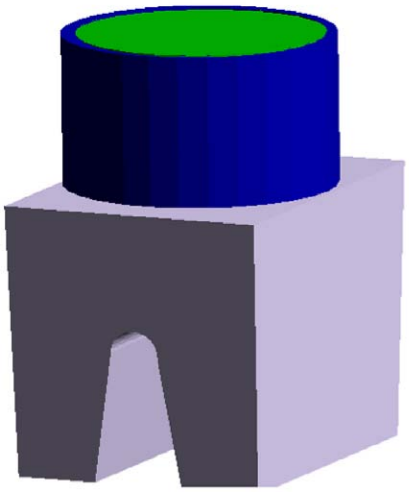

Figure 6. V-Block with riser and insulation

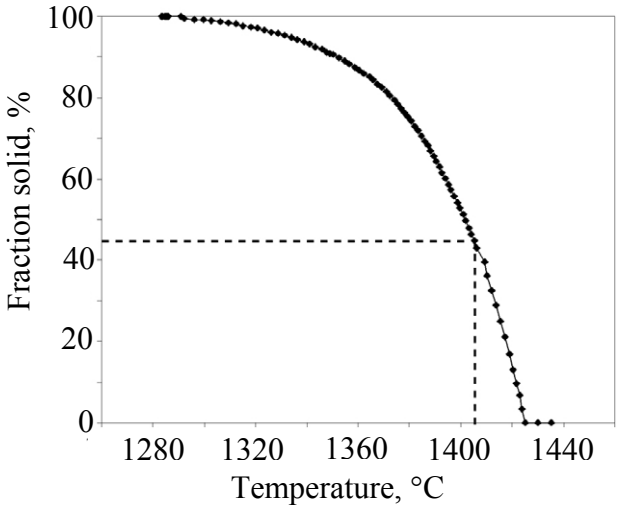

V-Block Baseline Information
Steel: CF-8M (same family of steel as trials, CF-8C)
Mold Sand: Furan
Simulation Start Temperature: 1500°C
Liquidus: 1425°C
Solidus: 1291°C
Critical Temperature: 1405°C (corresponds to 45% solid)
Interfacial Heat Transfer Coefficient: 1000 W/m^{2}K
Pour Weight: 69 kg

Figure 7. Left: Fraction of solid curve for CF-8M stainless steel; the dashed lines indicate the fraction solid corresponding to the critical temperature chosen for the baseline case. Right: Baseline simulation parameters for the V-block parametric studies.

Baseline Simulation Results. Figure 8 shows the burn-on and penetration predictions for the V-block corresponding to the baseline parameter values provided in Fig. 7. It can be seen that the predictions approximately coincide with the defect observed in the experiments (Fig. 5). All burn-on and penetration predictions are limited to the notch region. The predicted burn-on times on the casting surface increase toward the center of the notch, with the maximum value equal to 970 s. As expected, the predicted penetration times inside the mold decrease with increasing distance from the mold-metal interface. The maximum penetration time predicted is equal to 850 s. The depth and volume of sand predicted to be penetrated appears to compare well to the amount of penetrated sand visible in the experimental V-block section shown in Fig. 5.

In order to allow for a more quantitative comparison between the predictions and the measurements of Richards et al. [8], burn-on and penetration defect areas were determined from the simulation results in the following manner. The region on the casting surface where the burn-on time is predicted to be finite (i.e., above zero) represents the predicted burn-on area. As shown in Fig. 8, this area can be well approximated by a folded ellipse. The area of this ellipse was determined in the same manner as in the experiments of Richards et al. [8] (see the previous sub-section). The area on the mold surface where penetration is predicted to take place (i.e., where the penetration time is finite) was calculated in the same fashion. Note from Fig. 8 that the penetration area is somewhat smaller than the burn-on area, indicating the presence of considerable temperature gradients in the mold near the mold-metal interface. Since the depth of penetration into the mold was not measured, no comparisons were made with those predictions.

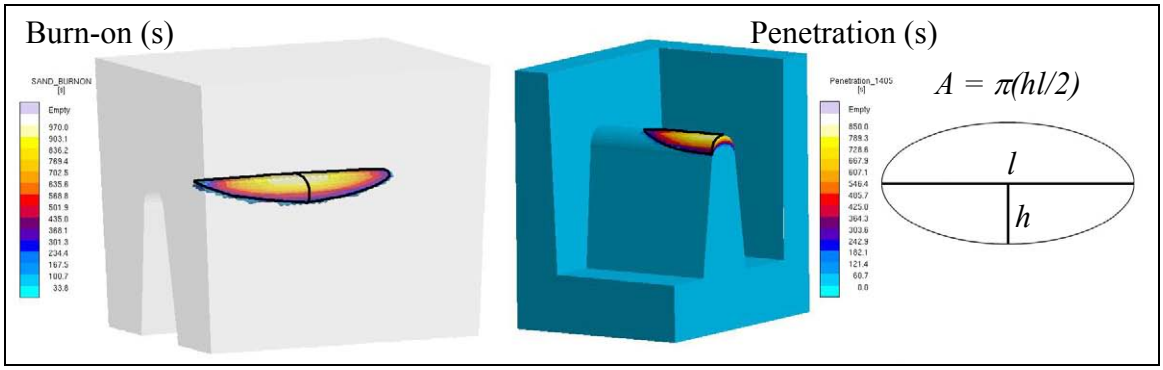

Figure 8. Predicted burn-on and penetration times for the V-block baseline case.

It should be mentioned that the present method of determining the burn-on and penetration areas for the V-block from the simulation results should be regarded as conservative. This is the case because all indications (within the region of interest) with finite burn-on or penetration times are included in the area calculations. The predicted areas would be somewhat smaller if, say, only the times above 100 s were included. Unfortunately, no information is available regarding the time necessary for burn-on or penetration to actually occur and a defect to form. In lieu of a more sophisticated model of the burn-on and penetration processes and considering the large scatter in the experimental data (see Tables 1 and 2), the present method of comparing the measured and predicted areas was deemed to be appropriate.

Parametric Study #1: Critical Temperature. For burn-on or penetration to occur, the steel must be above the temperature at which it is fully solid. In fact, at a sufficiently large fraction of solid, the liquid metal will not be able to flow anymore, and metal penetration into the mold will cease. Any solid fraction can be directly associated with a temperature, according to the solid fraction versus temperature curve for the steel under consideration (e.g., see Fig. 7). The critical temperature used for the burn-on and penetration predictions should, thus, be viewed as the temperature at which the solid fraction is large enough to inhibit liquid metal flow. In some casting simulation software, this critical solid fraction is referred to as the "feeding effectivity." Typical values range from 40% solid to 80% solid. Hence, the temperature corresponding to the feeding effectivity solid fraction can be used as a reasonable starting value for the critical temperature, as was done in the baseline case above.

In order to illustrate the sensitivity of the burn-on and penetration predictions to the choice of the critical temperature, and to validate the present method, a parametric study was undertaken. Figure 9 shows the results of seven simulations in which the critical temperature was varied from the 100% solid temperature to the liquidus temperature. It can be seen that the predicted burn-on and penetration times and indications strongly increase with decreasing critical temperature. In fact, the predictions corresponding to critical solid fractions above about 85% can be considered unrealistic. For such high critical solid fractions (or low critical temperatures), large burn-on and penetration times are predicted even on the outer casting surfaces. For critical temperatures approaching the liquidus temperature, on the other hand, the predicted burn-on and penetration indications become very small, since the mold never reaches such high temperatures. The burn-on and penetration predictions corresponding to critical solid fractions between 45% (baseline) and 82% appear to most closely correspond to the experimental results in Fig. 5. Overall, the burn-on predictions can be seen to be more sensitive to the choice of the critical temperature than the penetration predictions.

A direct comparison between the measured and predicted burn-on and penetration areas is shown in Figs. 10 and 11, respectively. In these figures, the burn-on and penetration areas are plotted against the critical temperature (or the corresponding solid fraction). The measured data correspond to the averages listed in Table 2. They were shifted along the horizontal axis until the measured averages fell on the line corresponding to the predictions. This was done in an attempt to infer from the measured areas the correct critical temperature to use in the simulations. Since the measured areas vary considerably depending on the sand type and other experimental factors, only a range of critical temperatures can be identified that results in agreement between the measured and predicted burn-on and penetration areas. For the steel under consideration, this range can be seen to be between about 20^{o}C and 45^{o}C below the liquidus temperature. That temperature range corresponds to critical solid fractions between about 45% and 80%. The aggregate mean of all measured areas is best predicted for a critical solid fraction of approximately 55%, with the value being slightly lower in Fig. 10 (for burn-on) than in Fig. 11 (for penetration). For lower critical solid fractions (or higher critical temperatures), the predicted burn-on and penetration areas would become too low. For

higher critical solid fractions (or lower critical temperatures), the predicted areas can become unrealistically large, as already noted in connection with Fig. 9. Considering the large variations in the measured areas and the uncertainties in the simulation results, it seems most appropriate to conclude that any critical temperature corresponding to solid fractions between 45% and 80% provides reasonable burn-on and penetration predictions. Note that the baseline case critical solid fraction of 45% (see Fig. 7) falls at the lower end of this range.

Parametric Study #2: Interfacial Heat Transfer Coefficient. In the second parametric study, the heat transfer coefficient at the mold-metal interface was varied. Five different simulations were performed with interfacial heat transfer coefficients of 500 W/m^2K, 800 W/m^2K, 1000 W/m^2K, 1500 W/m^2K, and 2000 W/m^2K. The results are shown in Fig. 12. It can be seen that the predicted burn-on areas and times increase with increasing interfacial heat transfer coefficient. This can be explained by the mold surface reaching a higher temperature when the thermal resistance of the interfacial air gap is decreased. This increase in the burn-on and penetration areas and times is, however, relatively small. Therefore, within the range studied (500 W/m^2K to 2000 W/m^2K), the predictions are relatively insensitive to the interfacial heat transfer coefficient. Interestingly, the maximum predicted penetration times for the five simulations change more than the maximum predicted burn-on times. This indicates that penetration is more sensitive to the thermal resistance of the interfacial air gap. It should be mentioned that the penetration times in Fig. 12 were obtained with a relatively large integration time step of 50 s. Therefore, the predicted penetration times are only accurate to within 50 s (or about 5%).

Parametric Study #3: Simulation Starting Temperature. The initial temperature of the steel in the mold that was chosen for the baseline case simulation (1500°C; see Fig. 7) represents only a rough estimate of the actual temperature of the steel at the conclusion of the mold filling process, as noted previously. Therefore, the effect of the simulation starting temperature on the burn-on and penetration predictions was investigated in a third parametric study. Simulations for three different starting temperatures were performed: 1500°C (baseline), 1550°C, and 1600°C. The computed results are shown in Fig. 13. It can be seen that the simulation starting temperature does indeed play a significant role in the prediction of burn-on and penetration. For an increase in the starting temperature of only 100°C, the predicted burn-on and penetration time nearly doubles. Furthermore, the predicted penetration volume increases by more than a factor of two. These increases are caused by the mold being heated to a higher temperature when the steel is initially at a higher temperature. A higher simulation starting temperature obviously corresponds to a higher pour temperature in practice. Therefore, the present parametric study indicates that burn-on and penetration defects are sensitive to the pour temperature.

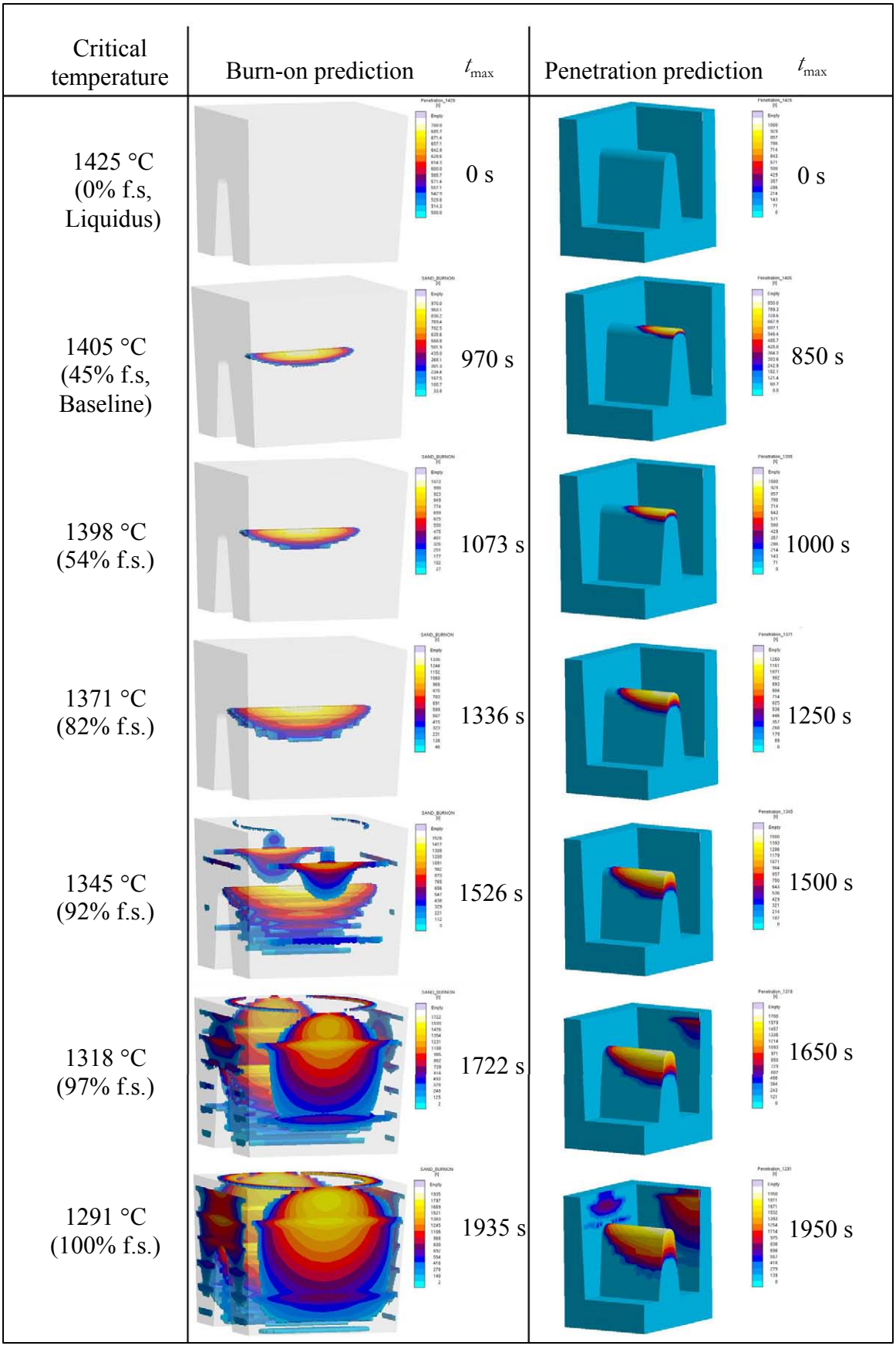

Figure 9. Parametric study #1: Effect of critical temperature on the burn-on and penetration predictions.

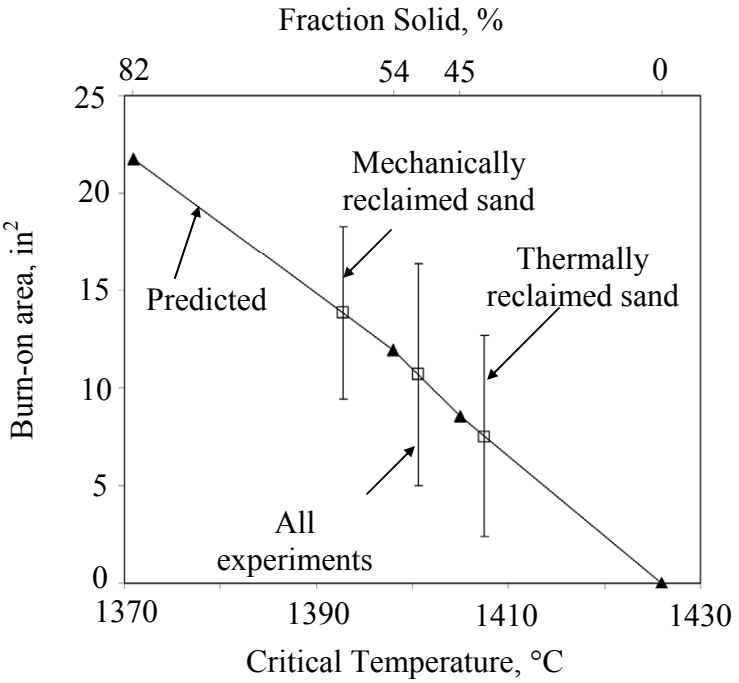

Figure 10. Variation of the predicted burn-on area with the critical temperature and comparison with experimentally measured areas.

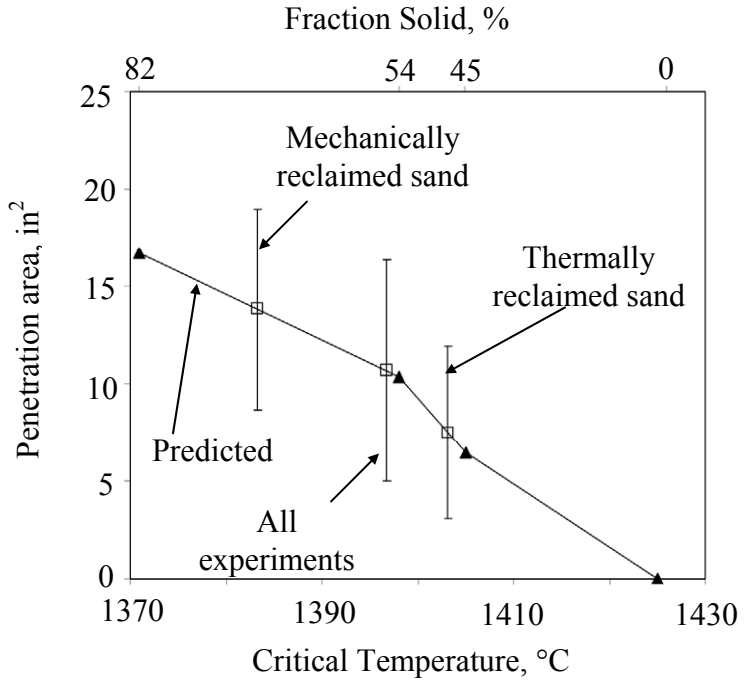

Figure 11. Variation of the predicted penetration area with the critical temperature and comparison with experimentally measured areas.

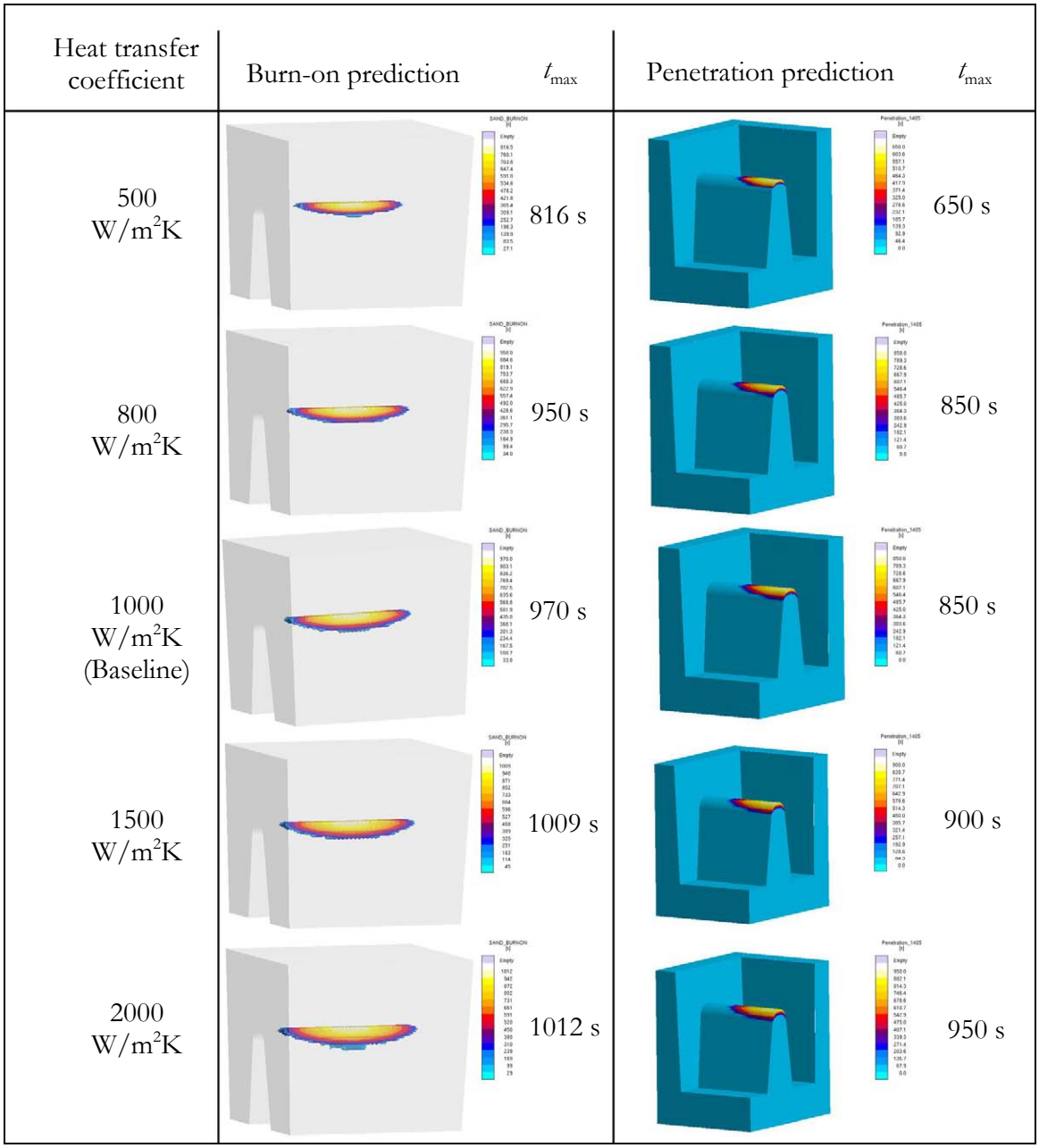

Figure 12. Parametric study #2: Effect of the interfacial heat transfer coefficient on the burn-on and penetration predictions.

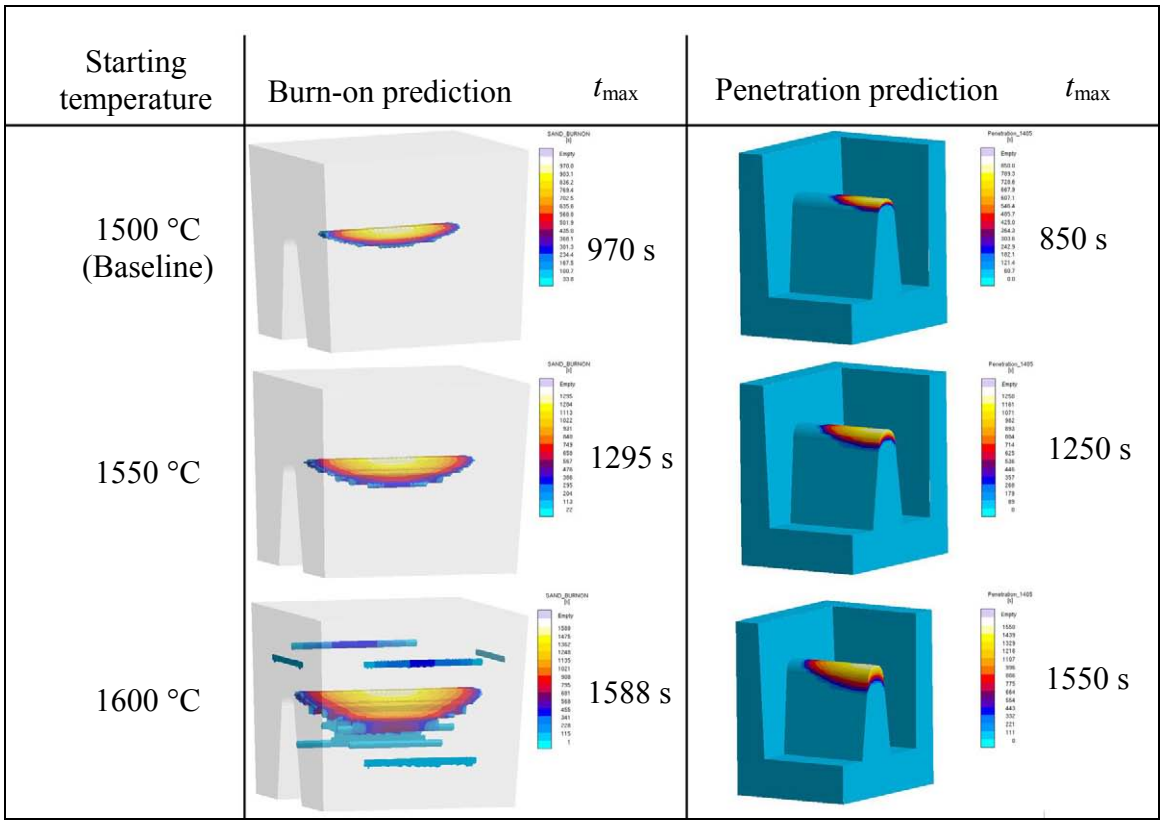

Figure 13. Parametric study #3: Effect of the starting temperature of the steel in the mold (filling was not simulated) on the burn-on and penetration predictions.

Parametric Study #4: Mold Material. The sensitivity of the present burn-on and penetration predictions to the type of mold material was investigated in a fourth parametric study. Five different sands were simulated: chromite, zircon, green, furan (PUNB, baseline), and dry silica. The thermo-physical properties for these mold materials are available in the database of the casting simulation software used. The computed results are shown in Fig. 14. It can be seen that the type of mold material plays a significant role in the prediction of both burn-on and penetration. Using chromite sand and, to a lesser extent, zircon sand results in the least amount of burn-on and penetration being predicted. In fact, no penetration is predicted for chromite sand. This can be expected due to the relatively high thermal conductivity of those two sands, which tends to lower the temperature of the mold. Chromite is often used in foundries as a facing sand to reduce burn-on and penetration defects. Comparing the other three mold materials (green, furan, and dry silica sand), Fig. 14 shows that furan has the least amount of burn-on area, but the largest penetration volume. For the dry silica sand mold, the most burn-on area and the longest penetration time are predicted. Overall, however, the differences in the burn-on and penetration predictions between these three mold materials are relatively minor.

Mold sand	Burn-on prediction	t_{max}	Penetration prediction	t_{max}
Chromite	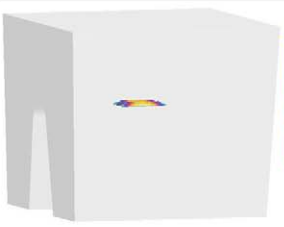	225 s	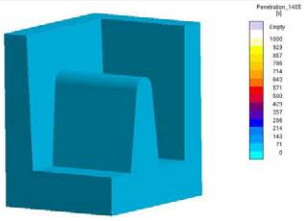	0 s
Zircon	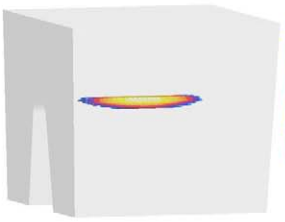	764 s	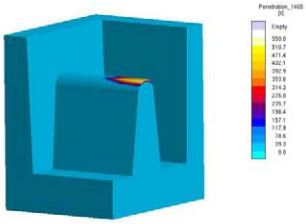	550 s
Green	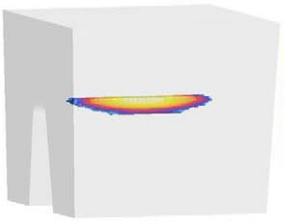	1008 s	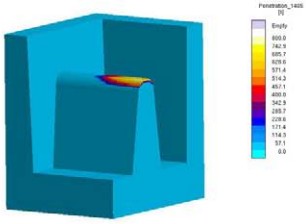	800 s
Furan (Baseline)	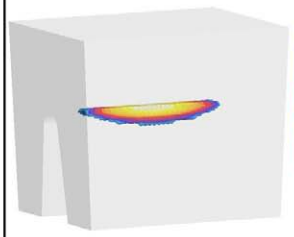	970 s	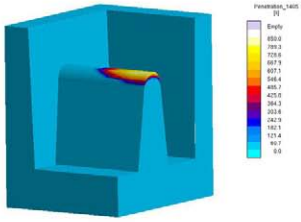	850 s
Dry silica	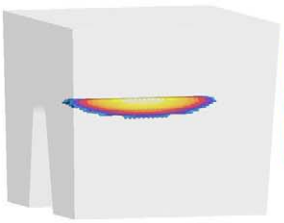	1154 s	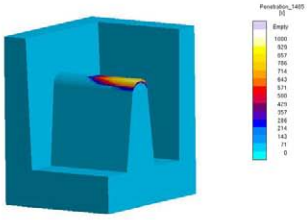	1000 s

Figure 14. Parametric study #4: Effect of the mold material on the burn-on and penetration predictions.

Case Studies

Three case studies were performed where burn-on and penetration predictions were compared to observations on actual production castings. All three castings are planetary gear casings made of low-alloy steel. The simulation setups for these case studies, including the values for all input parameters (pouring temperature, interfacial heat transfer coefficient, etc.) were provided directly by the foundries that produce these castings. No changes were made to the simulation setups. In all cases, the mold filling process was simulated. The critical temperature was set equal to the temperature that corresponds to the feeding effectivity solid fraction used by the foundries.

Case Study #1: Planetary Gear Casing A. The first case study performed was for the planetary gear casing shown in Fig. 15. The simulation parameters are also provided in Fig. 15, and the fraction of solid curve (for the GS30Mn5 steel) in Fig. 16. As shown in Fig. 17, the simulated half of this casting has a chromite core, a large riser at the top, and two small blind risers.

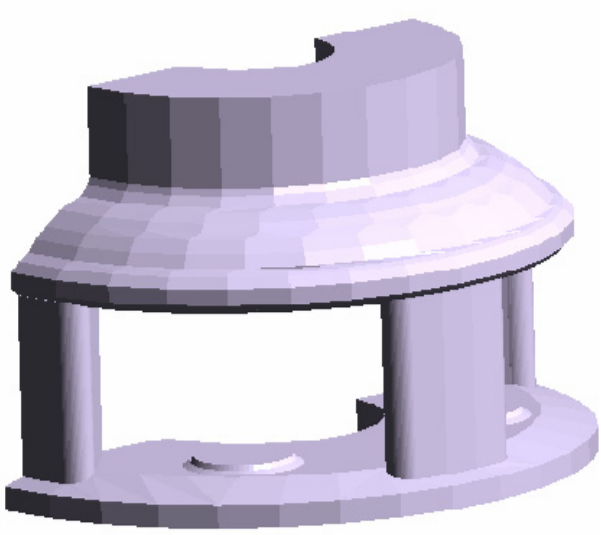

Case Study #1 Information
Steel: GS30Mn5
Mold Sand: Dry Silica Sand
Core: Chromite Sand
Pouring Temperature: 1600°C
Liquidus: 1498°C
Solidus: 1406°C
Critical Temperature: 1480°C
(corresponds to 45% solid)
Interfacial Heat Transfer Coefficient:
800 W/m^2K
Pour Weight: 5,964 kg

Figure 15. Left: picture of a symmetric-half of the planetary gear casing for case study #1. Right: simulation parameters.

The results of the burn-on predictions are shown in Fig. 18, together with a picture of the actual casting. A maximum burn-on time of 28,000 s is predicted, with numerous indications on both the inner and outer casting surfaces. No burn-on defects were observed on the actual casting. The reason for this disagreement is not entirely clear. Particularly large burn-on times are predicted on the upper part of the cylindrical inside surface. Presumably, the highly compacted chromite core adjacent to this surface prevented any burn-on defect from forming.

The penetration predictions are shown in Fig. 19. Penetration is predicted to occur *only* underneath the bottom blind risers. No penetration is predicted for the chromite core, indicating the presence of strong temperature gradients near the chromite core-steel interface. The penetration prediction for Case Study #1 is in complete agreement with the observations made on the casting, as shown in Fig. 19.

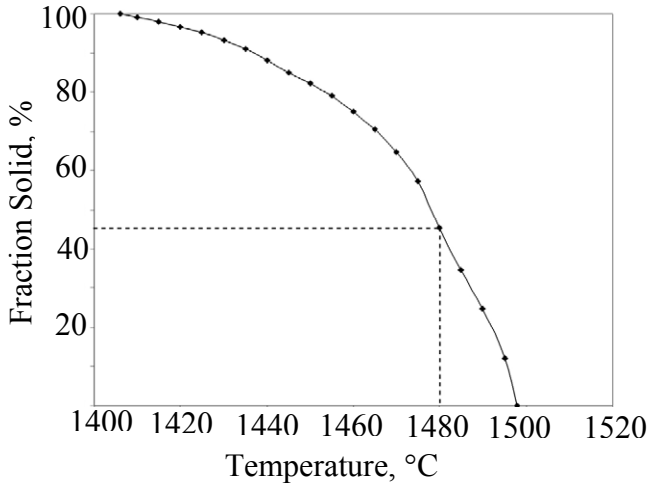

Figure 16. Left: Fraction of Solid curve for GS30Mn5 steel, marked at 45% solid, 1480 °C.

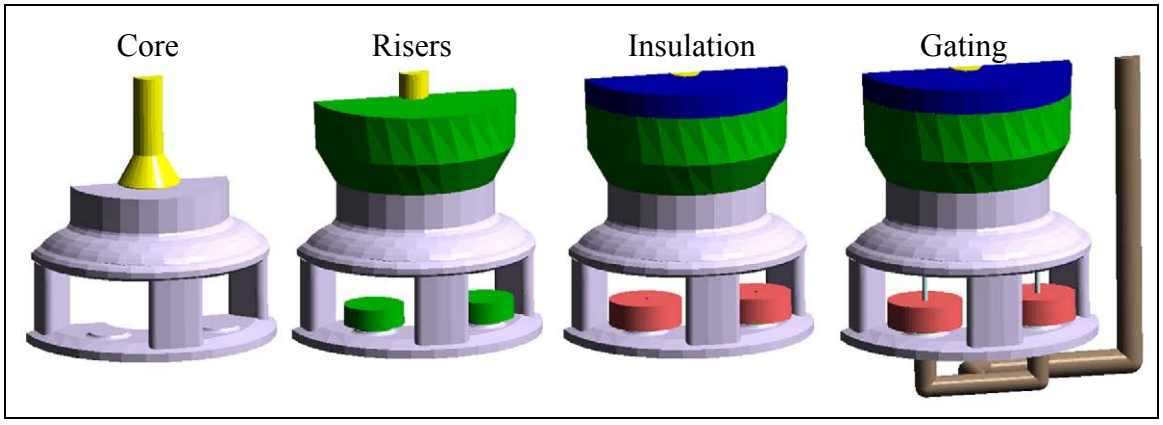

Figure 17. Four views of the casting for Case Study #1; the addition of each component of the casting is noted above the pictures.

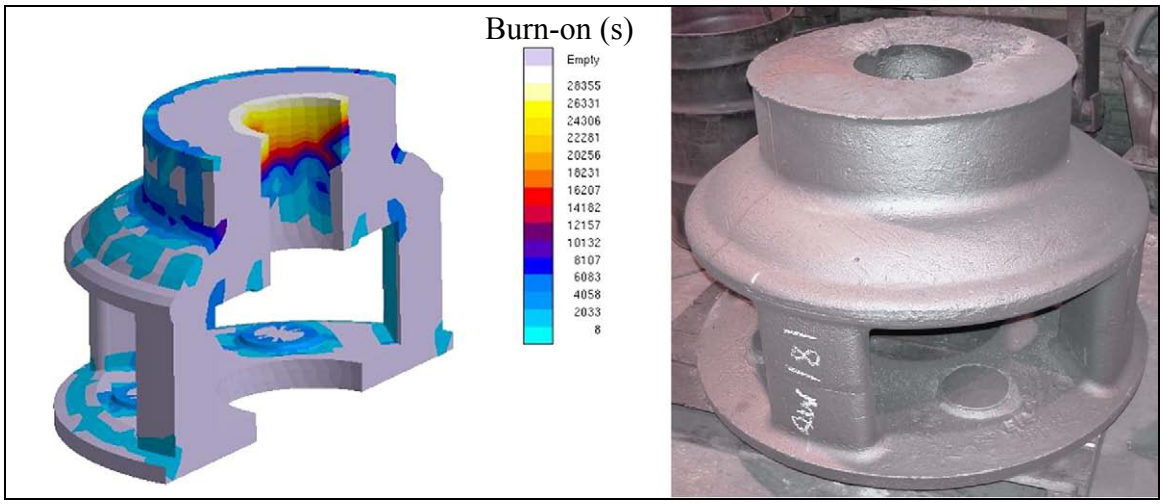

Figure 18. Comparison of predicted and observed burn-on defects for Case Study #1.

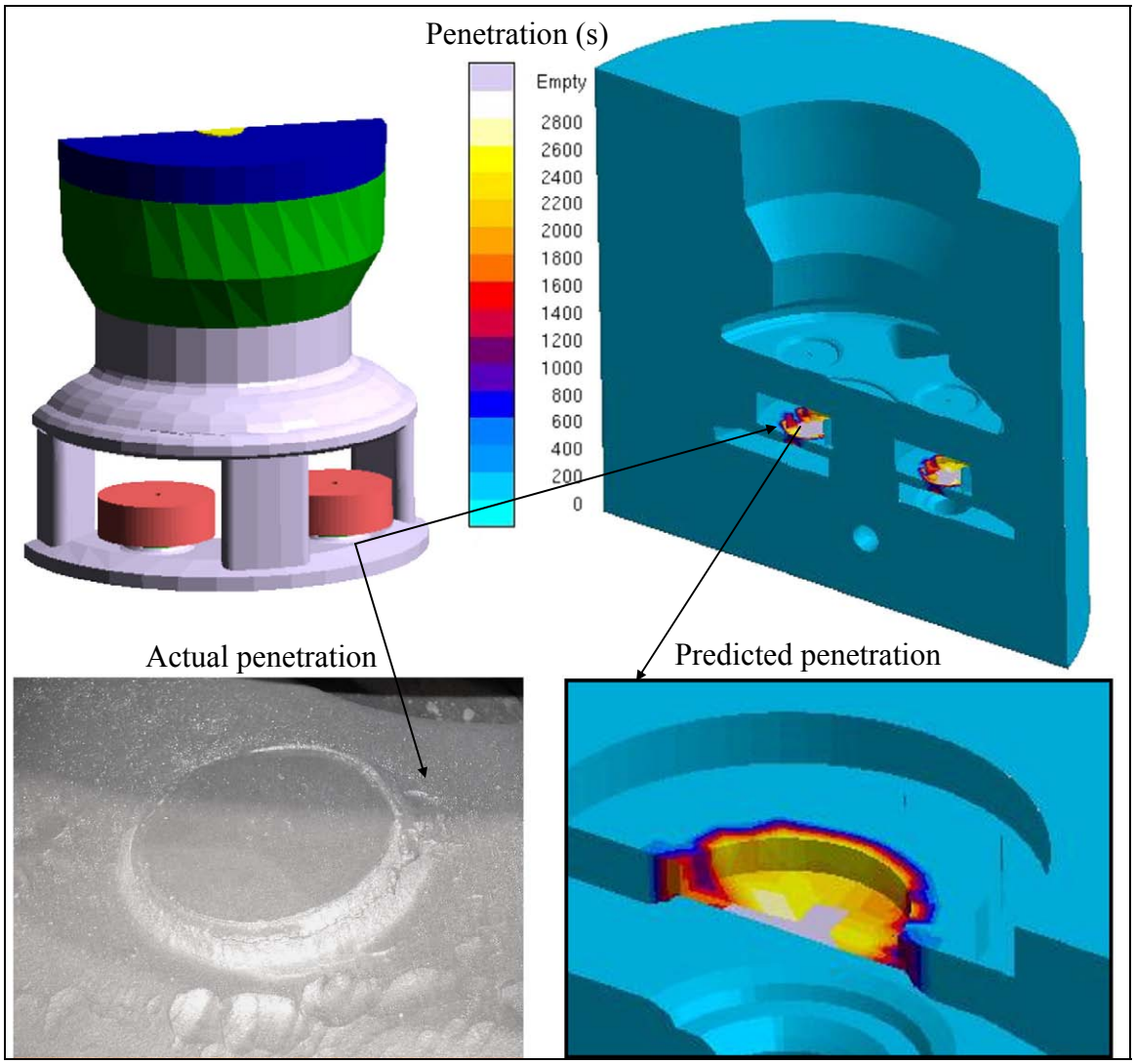

Figure 19. Comparison of predicted and observed penetration defects for Case Study #1.

Case Study #2: Planetary Gear Casing B. The second case study performed was again for a planetary gear casing; however, this casting was smaller and had significantly different rigging compared to the previous case study. A CAD drawing of the casting and the basic simulation parameters are provided in Fig. 20. The fraction of solid curve for the C19Mn5 steel from which the casting was made is shown in Fig. 21. This steel has a solidification temperature range of only 39°C, which is much smaller than the nearly 100°C range for the GS30Mn5 steel of Case Study #1. Moreover, the final 30% of the steel solidifies over a temperature range of less than 5°C. Presumably for these reasons, the feeding effectivity solid fraction was taken as 80% solid. As before, the corresponding temperature was taken as the critical temperature for the burn-on and penetration predictions. Thus, the critical temperature is only 36°C below the liquidus temperature for this steel.

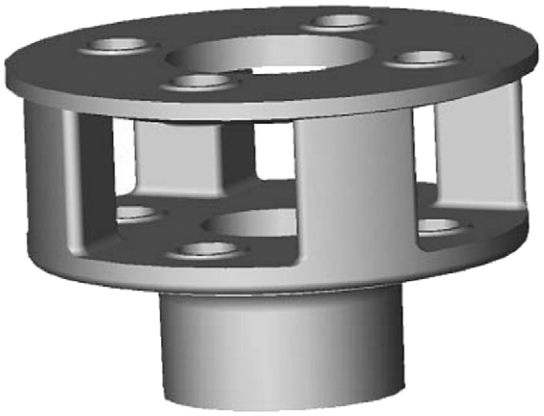

Case Study #2 Information
Steel: C19Mn5
Mold Sand: Furan and Chromite
Core: Furan and Chromite
Pour Temperature: 1580°C
Liquidus: 1501°C
Solidus: 1462°C
Critical Temperature: 1465°C
(corresponds to 80% solid)
Interfacial Heat Transfer Coefficient:
1,000 W/m^2K
Pour Weight: 3,484 kg

Figure 20. Left: CAD drawing of the planetary gear casing for case study #2. Right: simulation parameters.

An interesting aspect of this case study is that the final mold design was improved from its original design in order to reduce burn-on and penetration defects. During initial casting trials, several burn-on and penetration defects were observed on the outside surface of the casting. For subsequent castings, highly compacted chromite facing sand was added in those areas where the defects were most pronounced. The casting rigging, including the regions where chromite sand was added, is shown in Fig. 22. Therefore, this case study allows for an examination of the effect of the chromite facing sand.

The burn-on predictions for Case Study #2 are shown in Fig. 23, together with pictures of the actual casting. This figure corresponds to the case with chromite facing sand. The areas with the longest predicted burn-on times are (i) under the over-the-bore riser and (ii) in the corner of the junction near the bottom of the casting. All other indications are relatively minor. No chromite facing sand was added to the area under the over-the-bore riser, and this burn-on prediction agrees with the burn-on/penetration observations made on the casting (lower-left picture in Fig. 23).

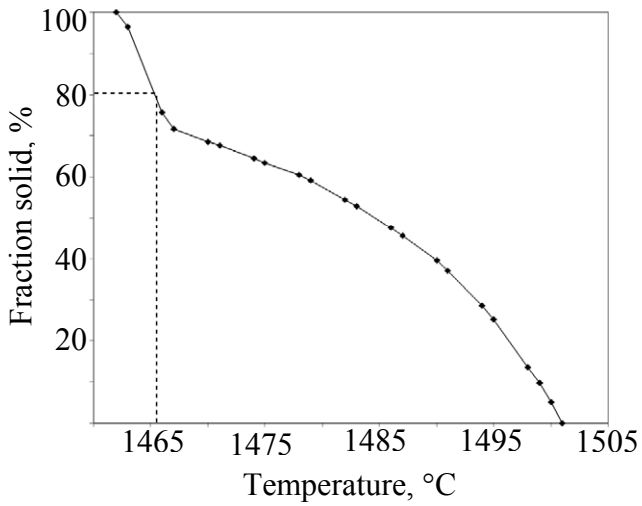

Figure 21. Fraction of solid curve for C19Mn5 steel, marked at 80% solid, 1465 °C.

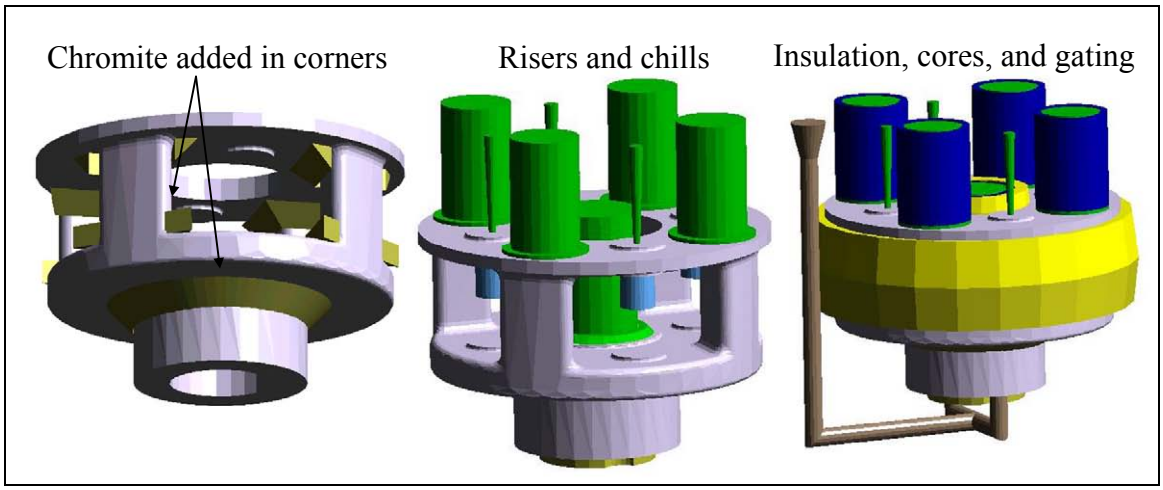

Figure 22. Three views of the casting for Case Study #2; the addition of each component of the casting is noted above the pictures.

For the actual casting, the addition of the chromite facing sand in the corner region did result in the elimination of the burn-on defect that was previously observed in this area. The slight surface indications that can be seen in the lower-right picture in Fig. 23 simply signify the extent of the chromite facing sand. Even though the chromite facing sand was included in the simulation, a burn-on defect is predicted to occur in the corner area. An additional simulation was conducted without the chromite facing sand, and the resulting burn-on predictions are compared to the case with chromite facing sand in Fig. 24. Although the maximum burn-on time is reduced by approximately 30% due to the addition of the chromite facing sand, the extent of the burn-on predictions in the corner is similar for the two cases. Therefore, the effect of the chromite facing sand is not adequately accounted for in the present burn-on simulation. It can be expected that the chromite facing sand in the corner region is highly compacted, which would lead to a significant increase in its effective thermal conductivity. Therefore, adjustments to the

thermal properties of the chromite facing sand could lead to better agreement between the burn-on observations and predictions.

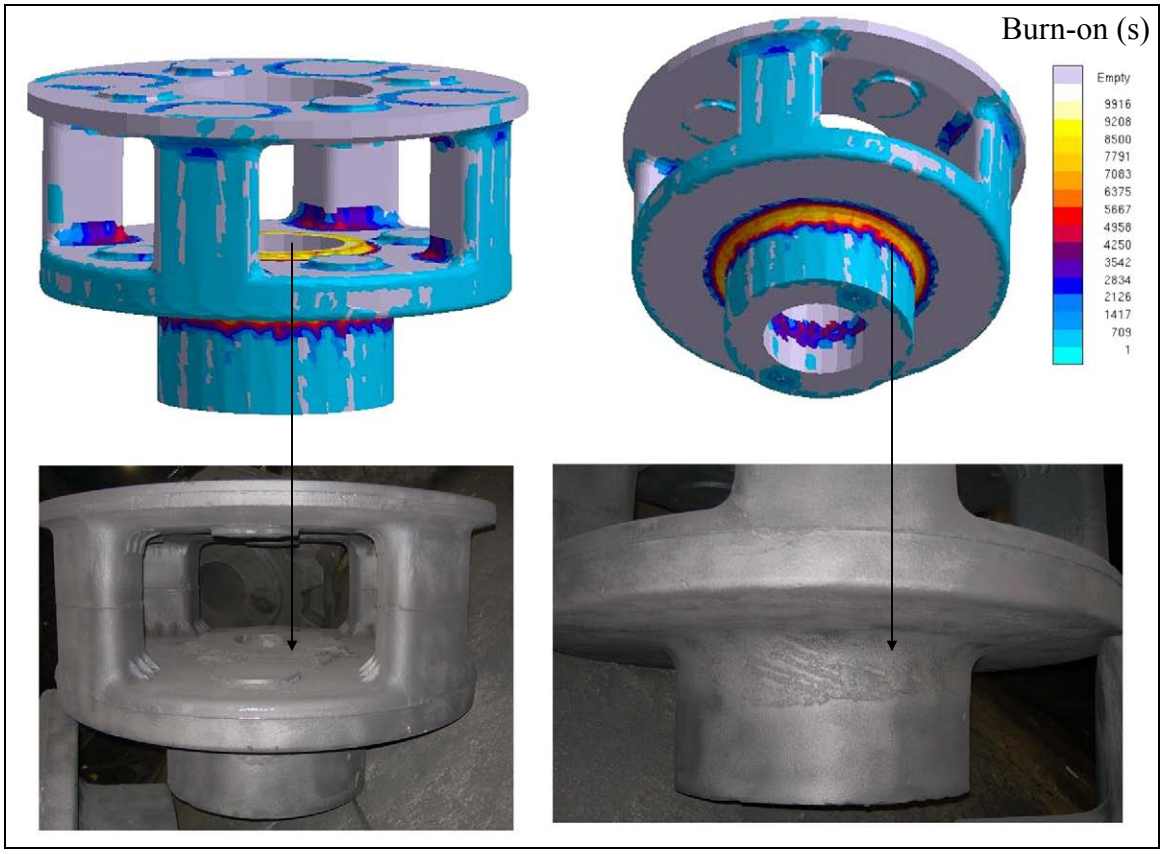

Figure 23. Comparison of predicted and observed burn-on defects for Case Study #2.

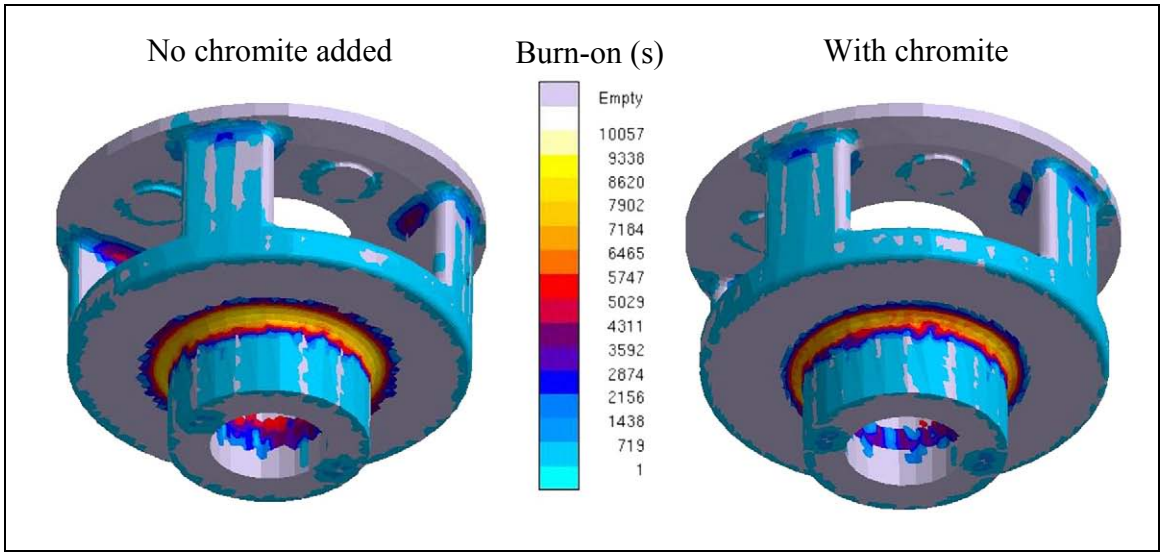

Figure 24. Effect of the addition of chromite facing sand on the predicted burn-on times for Case Study #2; the maximum burn-on time is reduced by approximately 30%.

The penetration predictions (with the chromite facing sand) for Case Study #2 are shown in Fig. 25. The *only* area where penetration is predicted is adjacent to the over-the bore riser. This is the same area for which a burn-on defect was predicted, as discussed in connection with Fig. 23. As shown in Fig. 25, this penetration (and burn-on) prediction is in agreement with the observations made on the actual casting. It is also worth mentioning that no penetration is predicted for the corner region where chromite facing sand was added. Therefore, as in Case Study #1, the penetration predictions are accurate.

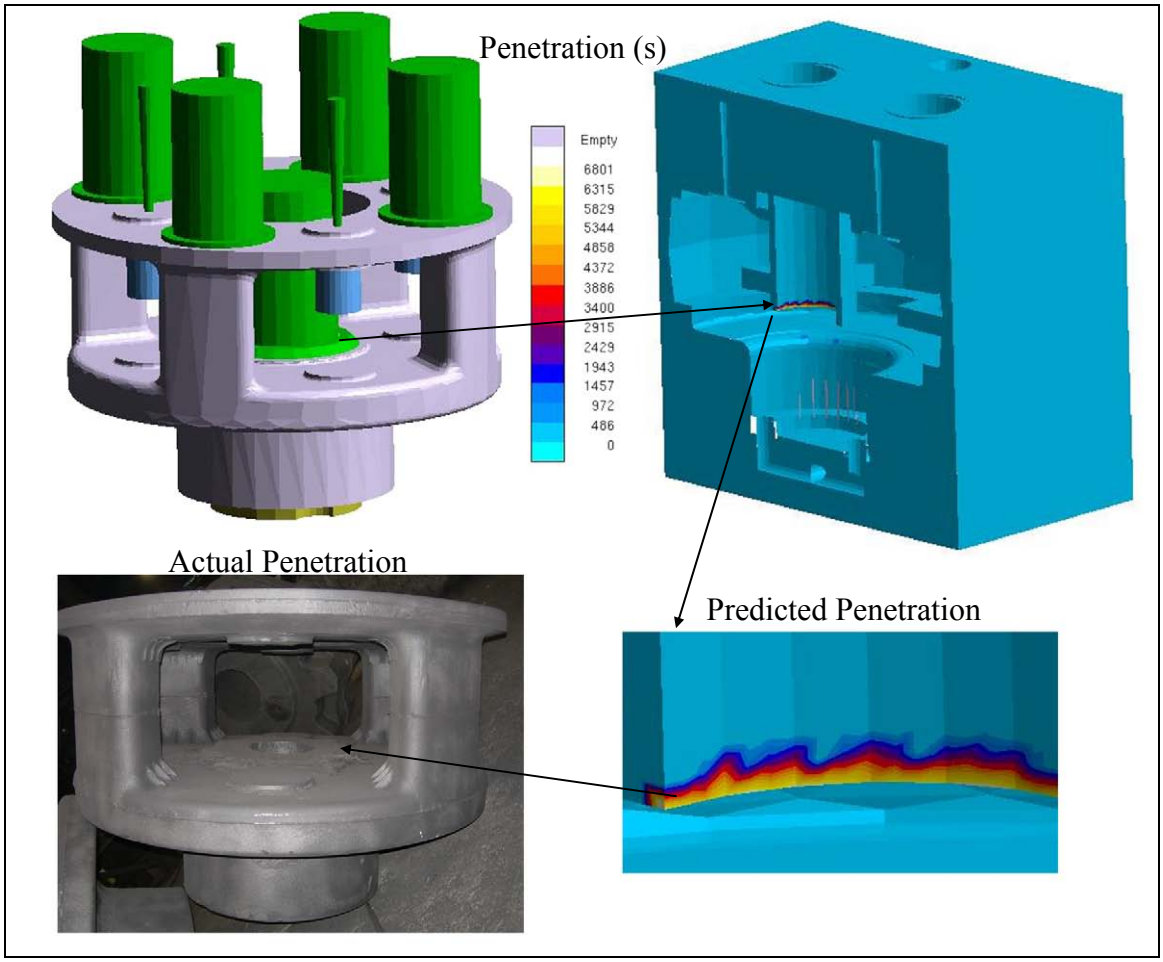

Figure 25. Comparison of predicted and observed penetration defects for Case Study #2.

Case Study #3: Planetary Gear Casing C. The third case study is also a large planetary gear casing made of C19Mn5 steel. A CAD drawing of the casting and the basic simulation parameters are provided in Fig. 26, while the rigging details are shown in Fig. 27. Chromite sand "rings" were added to the two external corners. These areas previously experienced burn-on defects.

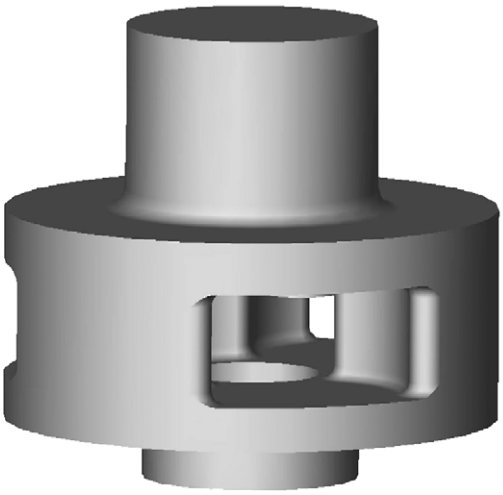

Case Study #3 Information
Steel: C19Mn5
Mold Sand: Furan and Chromite
Core: Furan
Pour Temperature: 1580°C
Liquidus: 1501°C
Solidus: 1462 °C
Critical Temperature: 1465°C (corresponds to 80% solid)
Interfacial Heat Transfer Coefficient: 1000 W/m^2K
Pour Weight: 2,559kg

Figure 26. Left: CAD drawing of the planetary gear casing for case study #3. Right: simulation parameters.

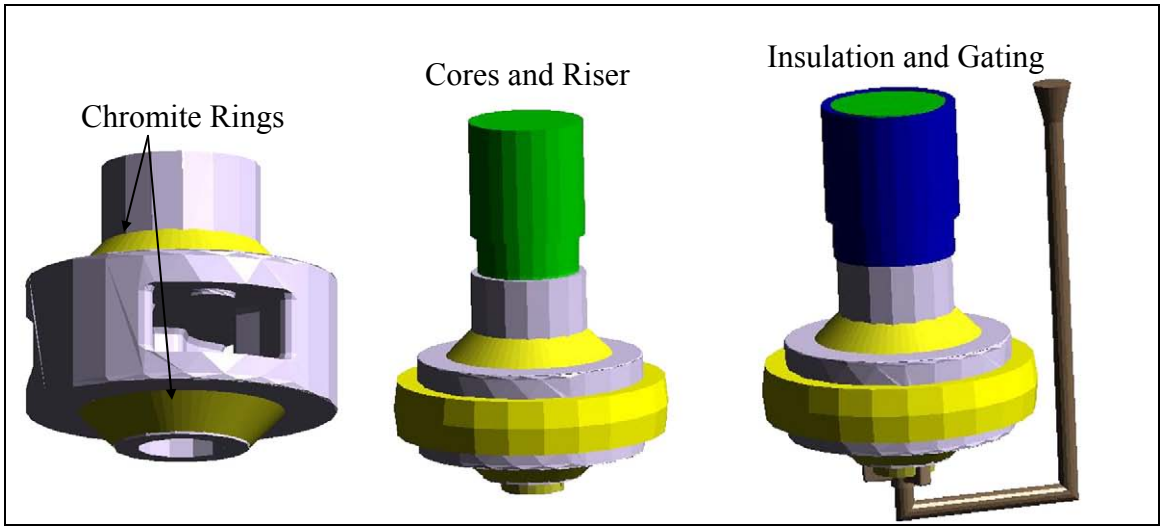

Figure 27. Three views of the casting for Case Study #3; the addition of each component of the casting is noted above the pictures.

A comparison of the predicted and observed burn-on defects for Case Study #3 (with chromite facing sand) is shown in Fig. 28. The predicted burn-on areas in the two external corners are not consistent with the observations on the casting. For the actual casting, the addition of the two chromite sand "rings" solved the burn-on problems in the

two external corners. As shown in Fig. 29, although the maximum burn-on times in these regions are reduced by approximately 20%, the simulation with the chromite sand "rings" still identifies these two locations as likely burn-on areas. This disagreement is similar in nature to that observed in Case Study #2: the effect of the chromite facing sand is not adequately accounted for in the present burn-on simulation.

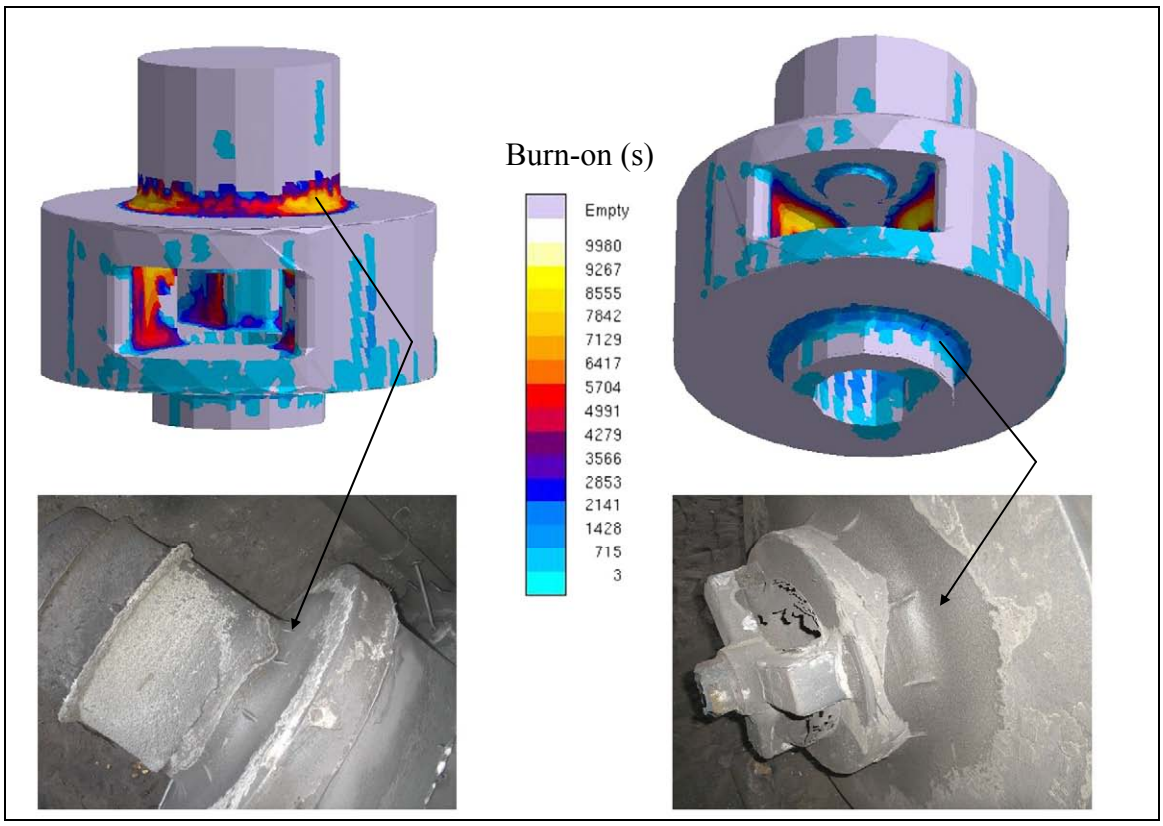

Figure 28. Comparison of predicted and observed burn-on defects for Case Study #3.

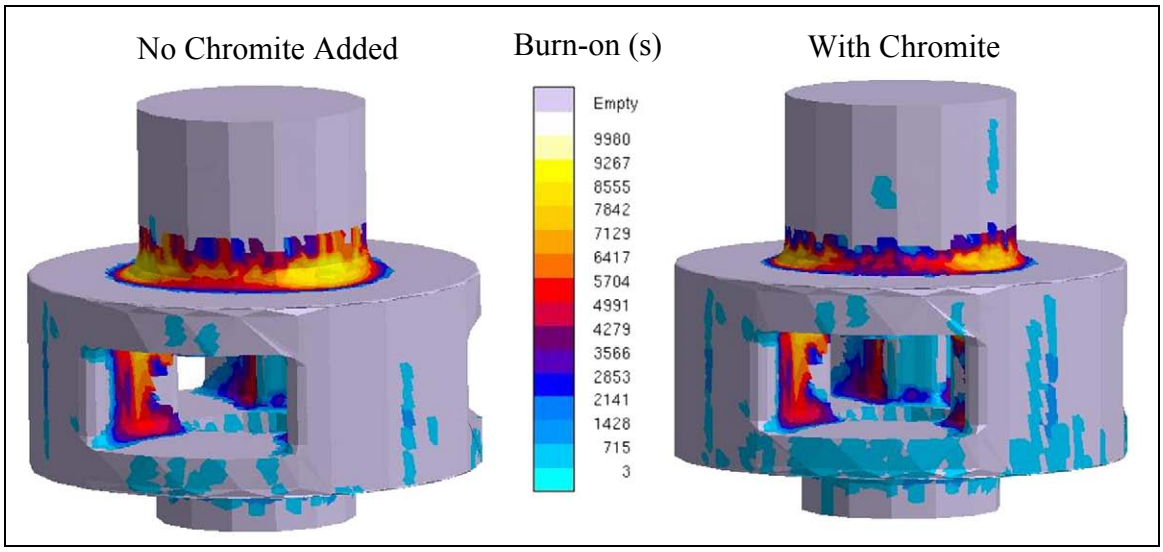

Figure 29. Effect of the addition of chromite facing sand on the predicted burn-on times for Case Study #3; the maximum burn-on time is reduced by approximately 20%.

As can be seen in both Figs. 28 and 29, another likely burn-on area is predicted on an internal casting surface, next to the thick section under the riser. No chromite sand was added in this location. Furthermore, Fig. 30 shows that penetration is predicted in the corners adjacent to the same internal casting surface. These burn-on and penetration predictions signify the same defect. They are in complete agreement with the observations made on the actual casting. A picture of this defect is included in Fig. 30. Therefore, as in Case Studies #1 and #2, the penetration predictions are accurate. Except for the effect of the chromite facing sand, the burn-on predictions can be considered accurate as well.

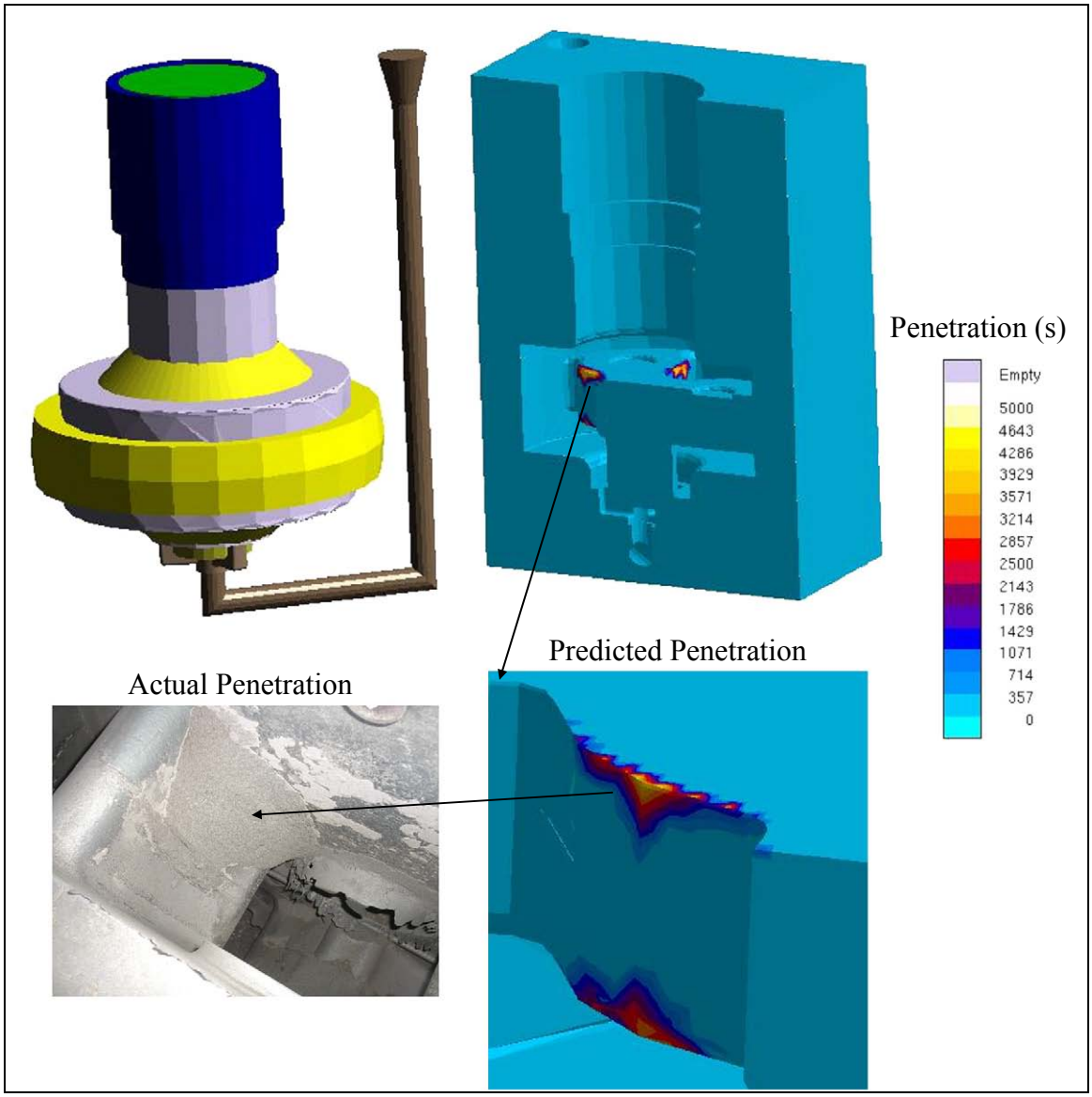

Figure 30. Comparison of predicted and observed penetration defects for Case Study #3.

Conclusions

A method was developed to predict likely areas of both burn-on and metal penetration casting surface defects. The method relies on the temperature predictions from a standard casting simulation, and calculates the times the mold-metal interface (for burn-on) and the mold (for penetration) temperatures are above a certain critical temperature. The present model was validated through comparisons with previous casting experiments involving a V-block [8]. Good agreement was achieved between the measured and predicted burn-on and penetration defect locations. By matching the measured and predicted defect areas, the critical temperature was determined to correspond to the temperature within the solidification range of the steel under consideration where the (critical) solid fraction is about 55%. However, realistic predictions were achieved for any critical solid fraction between 45% and 80%. Additional parametric studies were conducted to investigate the sensitivity of the predictions to the value of the interfacial heat transfer coefficient between the mold and the metal, the pouring temperature, and the type of molding material. These parametric studies indicate that the casting parameters in a simulation must be chosen carefully in order to closely match the conditions for the actual casting. Otherwise, burn-on or penetration defects may be vastly over- or under-predicted. The present method was further tested by performing case studies involving actual production steel castings that had burn-on and/or penetration defects. In all cases, the penetration predictions were in complete agreement with the observations made in the foundries. The burn-on predictions, on the other hand, were sometimes overly conservative and showed areas on the casting surfaces that did not actually experience a burn-on defect. In particular, the effect of chromite facing sand on the burn-on predictions deserves further attention. In applying the present method in foundry practice, it should be kept in mind that several of the factors that are known to affect burn-on and penetration defect formation are not taken into account. These factors include the metal head height, the type of sand reclamation, sand density, mold coating, and others. Nonetheless, the excellent accuracy of the penetration defect predictions should make the present method a valuable tool in the foundry industry.

Acknowledgements

The authors would like to acknowledge Dr. V.L. Richards of the University of Missouri for providing the experimental data, figures and other valuable information; and Mr. G. Hartay and Mr. J. Rondinelli of The Falk Corporation, and Mr. H. Davis, Mr. K. Pearl and Mr. D. Hoskins of the Sivyer Steel Corporation for their work and support with the case studies. Also, the authors would like to acknowledge Mr. R. Monroe of the Steel Founders' Society of America for suggesting this project, and his continued guidance throughout. Finally, the authors would like to thank Dr. M. Schneider and Magma Foundry Technologies for implementing the present method into their casting simulation software.

References

1. Glossary of Foundry Terms, http://www.atlasfdry.com/glossary.htm, The Atlas Foundry Company, Marion, IN, September 29, 2006.

2. Analysis of Casting Defects, Second Edition, American Foundrymen's Society, Des Plaines, IL, USA, 1966.

3. Richards, V.L., and Monroe, R., "Control of Metal Penetration in Steel Casting Production," in Proceedings of the Steel Founders' Society of America 52nd Annual Technical and Operating Conference, Chicago, IL, November, 1999.

4. Svoboda, J.M., and Gieger, G.H. "Mechanisms of Metal Penetration in Foundry Molds," AFS Transactions, Volume 77, pp. 281-288, 1969.

5. Stefanescu, D.M., and Giese, S., "Cast Iron Penetration in Sand Molds, Part I: Physics of Penetration Defects and Penetration Model," ASF Transactions, Volume 104, pp. 1233-1248, 1996.

6. Stefanescu, D.M., and Giese, S., "Cast Iron Penetration in Sand Molds, Part II: Experimental Evaluation of Some Main Parameters Responsible for Penetration," ASF Transactions, Volume 104, pp. 1249-1257, 1996.

7. Pattabhi, R., Lane, A.M., and Piwonka, T.S., "Cast Iron Penetration in Sand Molds, Part III: Measurement of Mold-Metal Interfacial Gas Composition," AFS Transactions, Volume 104, pp. 1259-1264, 1996.

8. Richards, V.L., Lekakh, S., and Kruse, B., "Burn-in/Burn-on: Coating Characterization and Designed Experiments," in Proceedings of the Steel Founders' Society of America 57th Annual Technical and Operating Conference, Chicago, IL, November 2004.

9. Richards, V.L., and Rasquinha, D.J., "Burn-in/Burn-on Case Study Findings," in Proceedings of the Steel Founders' Society of America 55th Annual Technical and Operating Conference, Chicago, IL, November 2002.

10. Richards, V.L., "Burn-in Burn-on: A Fertile Area for Research," in Proceedings of the Steel Founders' Society of America 54th Annual Technical and Operating Conference, Chicago, IL, November 2001.